



Solar-activated tin oxide photocatalysis for efficient naphthenic acids removal and toxicity reduction in oil sands process water

Hadi Mokarizadeh^a, Isaac Sánchez-Montes^a, Sunanda Paul^b, Nora A.S. Hussain^b, Kareem Moghrabi^b, James L. Stafford^b, Mohamed Gamal El-Din^{a,*}

^a Department of Civil and Environmental Engineering, University of Alberta, Edmonton, AB T6G 1H9, Canada

^b Department of Biological Sciences, University of Alberta, Edmonton, AB T6G 2E9, Canada

ARTICLE INFO

Keywords:

Solar-driven catalysis
Fluorophore organic contaminants
Classical NAs
Steady-state concentration of hydroxyl radicals
Immunotoxic effects

ABSTRACT

This research studied, for the first time, the effect of activating tin oxide (SnO₂) under simulated solar light for treating real oil sands process water (OSPW). The solar/SnO₂ system effectively eliminated fluorophore organic contaminants, classical naphthenic acids (O₂-NAs), and oxidized NAs (Oxy-NAs) from OSPW. The best experimental conditions to remove over 90 % of O₂-NAs were found to be 0.5 g/L SnO₂ under 8 h of irradiation. HO[•] and O₂^{•-} species identified by electron paramagnetic resonance (EPR) analysis played an important role in the degradation of NAs and other contaminants in real OSPW. The initial toxic effects of untreated OSPW were noticeably reduced after treatment, with a reduction of approximately 50 % in acute toxicity using Microtox® bioassay and over 80 % in the level of bioavailable hydrocarbons. In addition, the process also demonstrated a significant reduction in immunotoxicity as measured using an immune cell bioassay and reduced the toxic effects on *Staphylococcus warneri* using an adapted bacterial minimal inhibitory concentration (MIC) viability assay. These results suggest that treated OSPW by SnO₂ under solar light has high environmental compatibility, indicating it is safe for reuse in further applications.

1. Introduction

The extraction of bitumen from the oil sands in northern Alberta, Canada, results in the production of large volumes of oil sands process water (OSPW), an industrial effluent containing a diverse array of organic and inorganic compounds, most notably an abundance of naphthenic acids (NAs) and other organic contaminants [1–3]. The toxicity and potential risk of industrial process water, including OSPW, to human health and various organisms such as plants, fish, mammals, phytoplankton, zooplankton, and amphibians is one of the primary concerns [1,2]. This concern arises from the complex chemical composition of industrial process water, which contains residual bitumen, NAs, polycyclic aromatic hydrocarbons (PAHs), other organic compounds, and inorganic salts [4–8]. In particular, NAs contribute significantly to the toxicity of OSPW, as they are acutely toxic to a variety of organisms, particularly affecting reproductive physiology and endocrine function [9–11]. In addition, due to their surfactant characteristics, NAs can penetrate the cell walls of biological membranes [12,13]. Another

concern is the potential persistence of NAs in soil and water, with half-lives of 13 years or more [12,13]. Hence, treating OSPW is an important challenge in the oil sands industry.

Meanwhile, some treatment methods, including biodegradation, adsorption, and AOPs, have recently been recommended for treating OSPW. The low molecular weight NAs exhibit partial biodegradability and resistance to conventional wastewater treatment methods. Moreover, the persistence of heavier branched fractions underscores the need for advanced water treatment solutions in the reclamation of OSPW stored in tailings ponds [14–19]. Among AOPs, ultraviolet (UV)/H₂O₂, ozone-based, Fenton-based, and electrochemical-based processes have effectively removed synthetic and natural NAs. Nevertheless, their widespread application remains hindered by significant challenges, including high energy requirements, high chemical costs, the generation of harmful brominated by-products, and the requirement for acidic operating conditions [20–24], shifting the research attention toward more sustainable alternatives. In particular, the most prominent novel approaches to greener processes include the design of solar-driven

* Correspondence to: 7-285 Donadeo Innovation Centre for Engineering, Department of Civil and Environmental Engineering, University of Alberta, Edmonton, AB T6G 1H9, Canada.

E-mail address: mgamalel-din@ualberta.ca (M. Gamal El-Din).

<https://doi.org/10.1016/j.jece.2024.114168>

Received 25 June 2024; Received in revised form 23 August 2024; Accepted 16 September 2024

Available online 17 September 2024

2213-3437/© 2024 The Authors. Published by Elsevier Ltd. This is an open access article under the CC BY-NC-ND license (<http://creativecommons.org/licenses/by-nc-nd/4.0/>).

catalysts to reduce energy consumption and the use of low-cost and recyclable materials to lower operational and maintenance costs and environmental footprints [25,26].

To achieve a good performance degradation under solar irradiation, a catalyst should have proper valence band (VB) and conduction band (CB) positions, as well as an energy band gap (E_g), since these factors govern how well it absorbs light and generate electron-hole pairs (e^-/h^+) [27–29]. Different light sources, including UVA, UVC, and solar light, have been implemented in studies associated with photodegradation. Several studies focus on applying UV light as it possesses satisfactory energy to generate e^-/h^+ pairs within catalysts, leading to the generation of radicals and the subsequent degradation of pollutants [30,31]. However, UV-driven photodegradation consumes a high amount of energy.

Among different photocatalysts, tin oxide (SnO_2) is often characterized by its high oxygen vacancy capabilities, enhancing its properties as an n-type semiconductor to be activated under UV and visible light irradiation, despite having a relatively high E_g (3.6–4.0 eV) [32–34]. The high oxygen vacancy increases the availability of reactive sites, facilitates charge transfer, and reduces electron-hole recombination, leading to higher degradation rates [35]. Additionally, the position of the CB and VB of SnO_2 makes it a suitable catalyst for the formation of highly oxidizing radicals, especially hydroxyl (HO^\bullet) and superoxide (O_2^\bullet). This, coupled with its environmentally friendly and sustainable nature, makes this material worth investigating for OSPW treatment.

In this paper, we studied the performance of commercial SnO_2 nanoparticles activated under simulated solar radiation for the remediation of NAs and fluorophore organic compounds (FOCs) in real OSPW. While numerous studies have explored the application of solar-driven catalysts with different photocatalysts for degrading synthetic and industrial waste [36–38], as far as we know, there have been no previous works related to the application of SnO_2 for the degradation of NAs.

The main objectives of this work are to (1) evaluate the effectiveness and kinetics of SnO_2 photocatalysis in degrading NAs and FOCs in real OSPW, (2) identify the primary reactive oxygen species (ROS) involved in the degradation process, (3) evaluate the relative degradation of classical and oxidized NAs during the photocatalytic treatment, (4) study the impact of structural parameters, including carbon number and double bond equivalent (DBE) on the degradation of NAs, and (5) study the effectiveness of photocatalytic process in decreasing the toxicity of OSPW using different bioassays, including Microtox®, immunotoxicity based on inflammatory cytokine secretion levels, and bacterial viability.

2. Experimental

2.1. Chemicals and materials

OSPW utilized in the current work was sourced from a tailings pond in northern Alberta and stored in tightly sealed PVC containers at 4 °C. Before each use, the homogenized OSPW was filtered through an 8 μm PCTE filter. The properties of the used OSPW are presented in Table S1 in the supporting information file.

SnO_2 nanoparticles were supplied from Sigma-Aldrich and utilized without further purification. Ultrapure water (Millipore Synergy® UV) with a resistivity of $\geq 18.2 \text{ M}\Omega \text{ cm}$ was employed to prepare all solutions. 5,5-Dimethylpyrrolidine *N*-oxide (DMPO) and 2,2,6,6-tetramethylpiperidine (TEMP) were employed as trapping agents for the identification of HO^\bullet species and singlet oxygen ($^1\text{O}_2$), respectively.

2.2. Photocatalytic degradation experiments

Experiments were performed in batch operation mode utilizing a 100-mL borosilicate glass beaker. A solar simulator (SS200AAA, Photon Emission Tech; 1000 W ozone-free arc lamp) with a fixed irradiance of 112.53 W/m^2 was used in the photocatalytic experiments. The spectrum

of the solar radiation is shown in Figure S1, and a schematic representation of the experimental configuration is presented in Figure S2. In the photocatalysis experiment, SnO_2 nanoparticles in suspension were added at various concentrations to 50 mL of the OSPW and then steadily mixed (500 rpm) for 60 min under dark conditions to attain the adsorption equilibrium process. Afterward, the suspension was exposed to simulated solar radiation to start the experiment while continuously mixing throughout the treatment. Samples were taken at different intervals, filtered through a 0.2 μm filter, and then stored at 4 °C for subsequent analyses. Control experiments, including photolysis and experiments at dark conditions, were also performed.

2.3. Analytical procedures

The initial performance of the processes was assessed using synchronous fluorescence spectroscopy (SFS), a semi-quantitative technique for detecting FOCs, including certain NAs. SFS studies were conducted using a Varian Cary Eclipse fluorescence spectrophotometer with a fixed emission (218–618 nm) and excitation (200–600 nm) wavelength ranges. To conduct a more precise assessment of the concentration of NAs throughout the treatment, ultra-performance liquid chromatography coupled with quadrupole time-of-flight mass spectrometry (UPLC QTOF-MS) was employed to monitor the changes in NAs concentration (the detailed analytical procedure is described in Text S1).

The reflectance of ultraviolet and/or visible light for the applied catalysts in the wavelength range of 200–800 nm was analyzed using UV-Vis diffuse reflectance spectra (DRS). Then, the direct and indirect E_g for SnO_2 were determined through a Tauc plot (Figure S3). EPR analyses were performed to detect the main ROS generated during the activation of SnO_2 photocatalysts under solar light (detailed information is provided in Text S2).

2.4. Toxicity evaluation

The complete toxicity analysis, which includes acute toxicity using the Microtox® bioassay, cytokine analysis via the human macrophage cell line (THP-1) and the murine macrophage cell line (RAW 264.7), and microbial viability assay analysis using *Staphylococcus warneri* (*S. warneri*), was performed in this work. The details are available in Text S3.

3. Results and discussion

3.1. Performance in degrading fluorophore organic compounds (FOCs)

Real OSPW contains a variety of FOCs (molecules with fluorescence properties) with distinct chemical and toxic properties. SFS involves the simultaneous detection of emission and excitation scans, with a fixed wavelength difference ($\Delta\lambda$) between the two, and the multiplication of these signals. The chosen $\Delta\lambda$ determines the resulting signal, producing a narrow, single fluorescence band with a peak wavelength specific to the compound [39]. Typically, the compounds with aromatic groups and low-energy $\pi \rightarrow \pi^*$ transitions exhibit the highest fluorescence intensity in SFS analysis. However, alicyclic carbonyls, aliphatic, highly conjugated double-bond compounds, and PAHs found in OSPW can also exhibit fluorescence. While not providing quantitative measurements of these compounds, SFS analysis offers insights into the effectiveness of a treatment method in reducing mentioned contaminants.

First, control experiments were performed to measure their impact on the intensity of FOCs using simulated solar light and 0.1, 0.5, and 1.0 g/L of SnO_2 under dark conditions. In raw OSPW, the SFS signal of FOCs exhibits three peaks, i.e., a single-ring peak at approximately 272 nm, a two-fused rings peak at around 310 nm, and a three-fused rings peak at approximately 325 nm (Fig. 1). Single-ring aromatic compounds are predominant over two- and three-ring compounds, which is consistent with the literature [40,41].

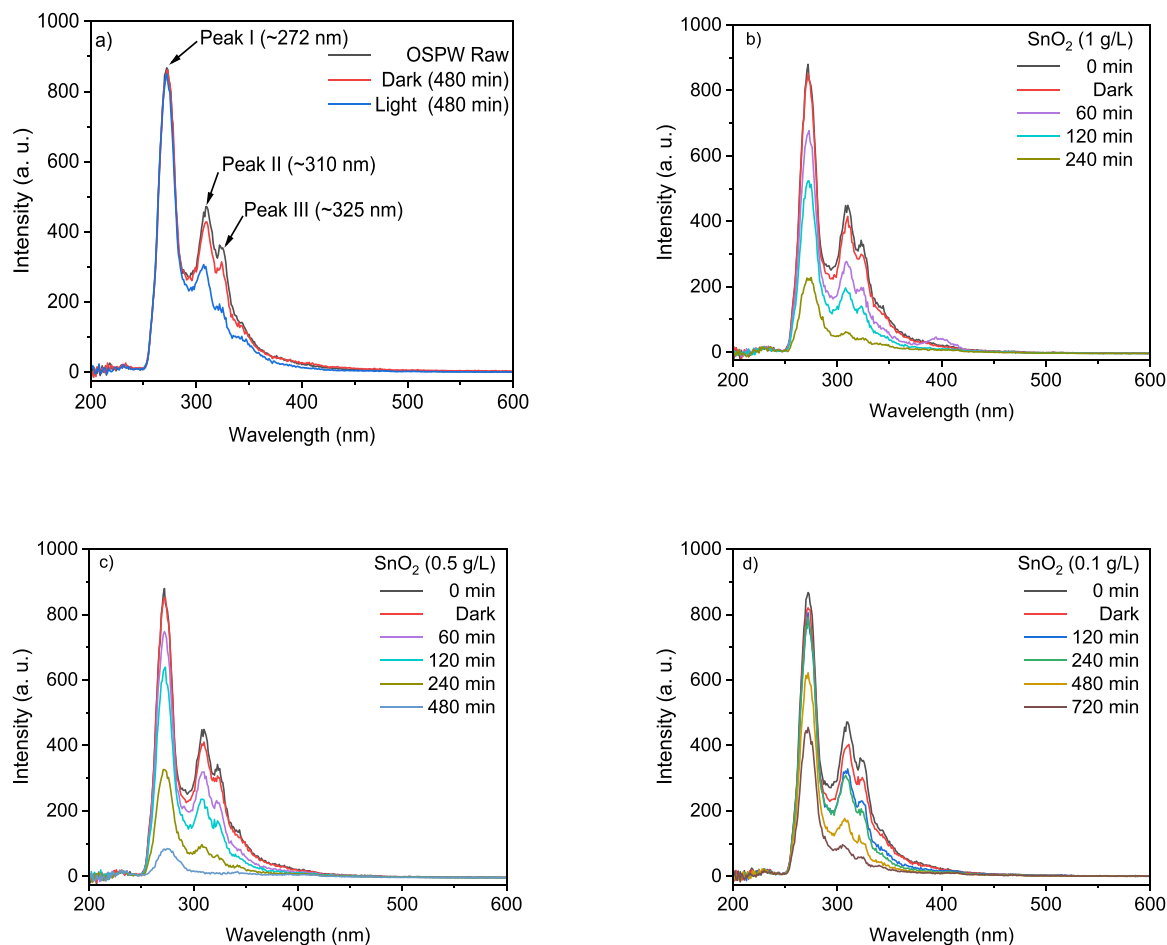


Fig. 1. Effect of SnO₂ photocatalyst under dark conditions and solar light on the signal of FOCs in OSPW: a) photolysis; b) 1.0 g/L of SnO₂; c) 0.5 g/L of SnO₂; d) 0.1 g/L of SnO₂. Experimental conditions: dark condition = 60 min; solar irradiance = 112.53 W/m²; and pH = 8.32.

Fig. 1a shows no significant removal rate within 8 h of irradiation using only the simulated solar light. This suggests that organics in untreated OSPW exhibit a limited absorption capacity for solar radiation, consistent with previous works [40,42]. Other authors have demonstrated that real OSPW presents a relatively high absorption of UV light, particularly in the specific range (240–320 nm). This leads to the breaking of chemical bonds within the FOCs, decreasing the fluorescence intensity in the SFS spectrum [41]. Moreover, a very low removal rate was observed under dark conditions, confirming the limited adsorption of organic contaminants in raw OSPW on SnO₂ nanoparticles. After the combination of SnO₂ particles with solar irradiation (Fig. 1b to Fig. 1d), the intensities of all three peaks decreased (particularly for two- and three-ring fused aromatic compounds), which could be associated with the breakage of chemical bonds in FOCs due to the generation of radicals resulting from the activation of SnO₂ to solar light. This selectivity is rooted in fused-ring aromatics containing sites with high electron density, making them prone to oxidative attack [43]. The significant decrease in peak intensities can primarily be ascribed to the effective activity of SnO₂ under solar light irradiation, demonstrating the high potential of solar-driven SnO₂ catalysts for the degradation of NAs in real OSPW.

The kinetics of the mentioned aromatic groups were solely evaluated for the SnO₂ catalyst at the best condition (0.5 g/L) after 8 h by correlating their relative intensities. As shown in Figure S4, the findings reveal that the removal rate across the groups increases with the increase in the number of fused rings. This outcome aligns with expectations from the oxidation reactions of aromatic compounds, where a higher number of fused rings cause a greater density of readily available

electrons for oxidative chemical attacks [44]. HO[•] species are recognized for their ability to react with aromatic moieties through electrophilic addition reactions on the aromatic rings and hydrogen atom abstraction at the branches. These reactions can lead to either the loss of aromaticity due to aromatic ring opening or the weakening aromaticity due to the introduction of electron-withdrawing groups onto or near the aromatic rings [45].

3.2. Performance in the degradation of NAs

O₂-NAs degradation was evaluated during the photocatalytic treatment using SnO₂ nanoparticles under solar light. As depicted in Fig. 2a, approximately 80 % of the O₂-NAs were removed after 4 h of treatment with 1.0 g/L of catalyst. The experiments were repeated with 0.5 g/L of SnO₂ to adjust the initial catalyst concentration while increasing the irradiation time to 8 h, as illustrated in Fig. 2b. In this case, the degradation of O₂-NAs exceeded 90 %, suggesting that the performance of the system can be adjusted by simply changing the SnO₂ dosage and the irradiation of simulated solar light. Given the importance of catalyst dosage for large-scale applications, 0.5 g/L of SnO₂ appears to be the most practical and effective concentration for this photocatalytic process. The main analytical analyses and toxicity evaluations were conducted under this condition. A dark control experiment (Fig. 2c) evaluated the cumulative adsorption over the same degradation period, showing a low contribution to classical NAs removal (approximately 10 %). This can be due to the relatively low surface area (29.185 m²/g) and limited adsorption capacity of SnO₂ (The BET analysis and SEM image of SnO₂ are displayed in Table S2 and Figure S5, respectively).

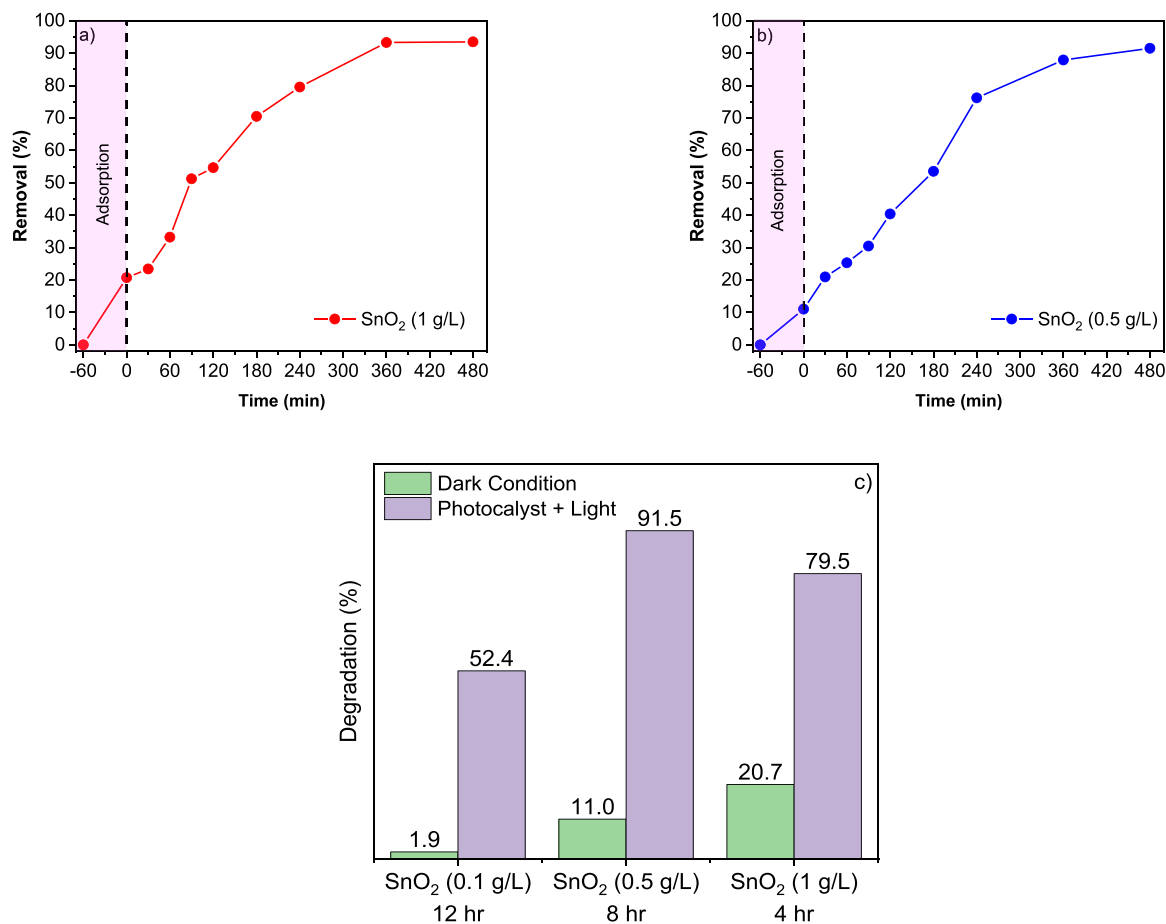


Fig. 2. Effect of SnO₂ photocatalyst under dark conditions and solar light on O₂-NAs removal present in OSPW. Experimental conditions: dark condition = 60 min; SnO₂ concentrations = 0.1, 0.5, and 1.0 g/L; solar irradiance = 112.53 W/m²; and pH = 8.32.

Moreover, the photolysis control experiment determined the degradation percentage of O₂-NAs under solar radiation. The results exhibited no substantial change in the initial concentration of NAs. This suggests that natural NAs in OSPW are stable to photolysis, consistent with previous reports on their high stability under solar light [46,47]. During the actual photocatalytic process, adsorption-based removal is anticipated to be minimal, as the majority of the adsorbed fraction would have undergone oxidation throughout the nearly complete change of NAs. Therefore, the principal removal mechanism for NAs would be ascribed to the photocatalytic activity of SnO₂. The concentration of NAs was tabulated for both classical and oxidized (oxy-NAs; O₃-, O₄-, O₅-, and O₆-NAs) forms of NAs in untreated OSPW (Table S1). O₂-NAs constituted more than half of the total NAs, with approximately 97 % associated with O₂-, O₃-, and O₄-NAs. So, O₃- and O₄-NAs arguably deserve more attention than O₅-NAs and O₆-NAs owing to their dominant abundance. In this case, the process efficiency at the best conditions was also analyzed for O₃- and O₄-NAs, as shown in Fig. 3.

The photocatalysis system showed a removal efficiency of 72.1 % and 54.7 % for O₃- and O₄-NAs, respectively, which was lower compared to the degradation of classical NAs (91.5 %). This behavior is likely linked to the engaged radicals in the oxidation mechanism of O₂-NAs, which could produce intermediates containing varied numbers of oxygen atoms. HO[•] species playing a vital role in photocatalysis could potentially yield hydroxylated by-products [41,48]. The behavior observed for oxidized NAs degradation aligns with findings from other AOPs such as ozonation, UV/H₂O₂, ferrate (VI) oxidation, UVA LED/PDS, and UVA LED/PMS [43,48–50]. The change in concentrations of oxidized NAs during the photocatalytic process is more complex to follow, as Oxy-NAs are simultaneously consumed and produced [22,43].

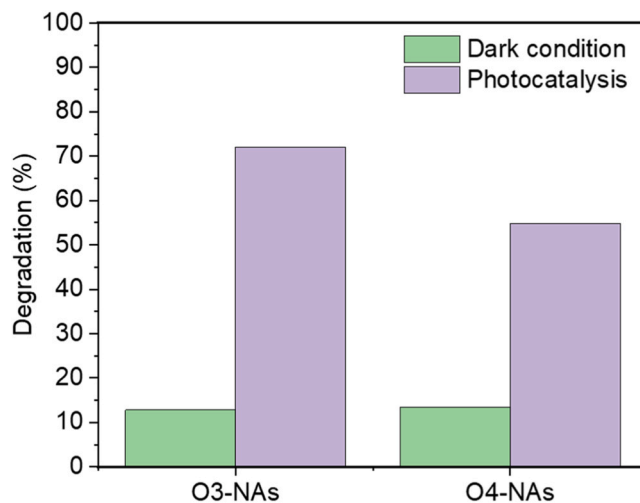
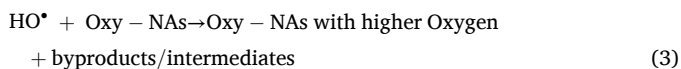
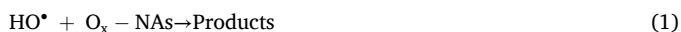


Fig. 3. Effect of SnO₂ photocatalyst under dark conditions and solar light for removing O₃- and O₄-NAs present in real OSPW. Experimental conditions: SnO₂ concentration = 0.5 g/L; dark condition = 60 min; solar irradiance = 112.53 W/m²; pH = 8.32; and treatment time = 8 h.

As confirmed in AOPs like ozonation, ferrate (VI) oxidation, and UV/H₂O₂, higher Oxy-NAs were generated from the oxidation of O₂-NAs and lower oxidized NAs, particularly at lower oxidant doses. This suggests that they were produced as intermediates of the oxidation process [43]. The hypothetical primary reactions for oxidation via the generated

HO• are as follows in Eqs. (1), (2), (3) [50]:



Thus, the involvement of HO• radicals in generating O_{x+1}-NAs species (where x ≥ 2) may contribute to the generation of oxidized NAs in the treated samples and subsequently result in their lower degradation. The findings of this work emphasize the significant promise of solar-driven SnO₂ catalysis in degrading NAs in OSPW. While commercial TiO₂ nanoparticles under simulated solar light with a fixed irradiance (277.92 W/m²) were employed by Suara et al. (2022) as a photocatalyst for treating real OSPW, their results revealed an approximate 60 % degradation of NAs after a 4 h reaction with a 1.0 g/L concentration of photocatalyst [40]. Some studies examined the effects of various solar-driven catalysts on degrading O₂-NAs in OSPW, as presented in Table 1.

3.3. Relative degradation of NAs as a function of double bond equivalents and carbon number

As is evident from the general formula of NAs, NAs have been categorized according to the degree of cyclicity quantified by DBE and the number of carbon atoms. Previous studies have confirmed that NAs with higher carbon numbers and increased cyclicity exhibit resistance to biodegradation, resulting in heightened environmental persistence [13, 16]. These recalcitrant NAs are known to demonstrate elevated hydrophobicity, leading to increased toxicity [52,53]. Furthermore, NAs with higher DBE values have been implicated in the estrogenic effects observed in raw OSPW [40,54]. Consequently, evaluating the NAs degradation efficacy based on DBE and carbon number is crucial. UPLC QToF-MS scanning of oxidized intermediates confirmed that the degradation process selectively targeted heavier and more cyclic NAs (compounds with a higher number of DBE). These compounds are the most environmentally persistent portions of NAs. The higher effectiveness of solar-driven catalysis using 0.5 g/L SnO₂ after 8 h in degrading NAs with higher DBE and carbon number was attributed to the presence of more oxidation sites (Figure S6). The observed trend agreed with previous studies, as processes (such as photocatalysis) favorably target branch points in NAs and other aliphatic contaminants [46,55].

3.4. Degradation kinetics of NAs

The degradation rate constants for classical NAs were examined via a pseudo-first-order kinetic model. Assuming no interference with active catalyst sites from undesired reactants and achieving a state of dynamic equilibrium at the interface between the solid catalyst and the liquid phase, the Langmuir-Hinshelwood (LH) kinetic model typically describes heterogeneous photocatalysis (Eq. 4). When integrated and applied at low concentrations of target reactants, this model changes to the pseudo-first-order form (Eq. 5).

$$-\frac{dC}{dt} = k_r \theta_s = \frac{k_r K C}{1 + K C_0} \quad (4)$$

$$\ln\left(\frac{C}{C_0}\right) = -k_r K t = -k_{app} t \quad (5)$$

Fig. 4 presents the degradation kinetics of O₂-NAs in OSPW using SnO₂ photocatalyst. The results confirm that the degradation of O₂-NAs is in good agreement with a pseudo-first-order reaction rate. However, it is important to note that the rate constants derived from Eq. 5 may deviate from their true values. The k_{app} values attained for classical NAs at concentrations of 0.5 and 1.0 g/L were 0.0055 and 0.0063 min⁻¹, respectively. While these constants provide useful insights for practical applications, they are apparent values and do not capture the nuanced complexities of the reaction kinetics of NAs. Yet, the relatively high k_{app} values found in the current work underscore the efficacy of the applied process for organic remediation in OSPW.

3.5. Detection of ROS and their roles in the degradation of classical NAs

HO• species were detected by EPR measurements employing DMPO as the trapping agent. This method results in an EPR-detectable radical adduct (DMPO•-OH), as presented in Figure S7 [56–58]. The analysis of EPR spectra for the detection of HO•, O₂^{•-}, and ¹O₂ species in SnO₂ solution under solar light is depicted in Fig. 5. The EPR spectra showed two groups of peaks observed during the SnO₂ activation: i) a group of four equally spaced intense peaks (*) with a rough ratio of 1:2:2:1, characteristic of the DMPO•-OH adduct (Fig. 5a) and ii) four peaks derived from O₂^{•-} (+) with a rough ratio of 1:1:1:1 (Fig. 5a). In this sense, the observed signals suggest that both HO• and O₂^{•-} and species are involved in the degradation mechanism of NAs. It is worth mentioning that no EPR signals were detected on the SnO₂ photocatalyst in dark conditions, confirming that the formation of ROS required light excitation.

EPR measurements also investigated the generation of the non-radical ¹O₂ by utilizing TEMP as a trapping agent. TEMP can generate the spin-adduct TEMP-¹O₂ in the presence of ¹O₂ species [59,60]. Generally, three-line signals with a rough ratio of 1:1:1 indicate ¹O₂ formation on the surface of the photocatalyst under light irradiation [61]. As depicted in Fig. 5b, the EPR analysis of the activated photocatalyst showed nearly comparable signal intensities in the three equidistant peaks typical of TEMP-¹O₂, which were similar to those observed in the control experiment. This indicates that there was no substantial generation of ¹O₂ during the activation of SnO₂, confirming their minor role in the degradation process. Thus, the effective degradation of NAs under solar light is ascribed mainly to the presence of HO•, followed by a secondary role of O₂^{•-} species.

3.6. Quantification of HO• using TA as a chemical probe

Quantifying HO• is essential for evaluating the effectiveness of AOPs. However, directly measuring HO• concentration is challenging owing to their high reactivity and short lifespan (~10⁻⁶ s) [62]. To overcome this, indirect techniques like emission spectroscopy, laser-induced fluorescence, and chemical probes are used [63–68]. Chemical probes, such as terephthalic acid (TA), offer a cost-effective and relatively quick

Table 1
Performance of different photocatalysts in degrading O₂-NAs in OSPW.

Photocatalyst	Band Gap (eV)	Best dose / time	Total NAs (mg/L)	O ₂ -NAs (mg/L)	O ₂ -NAs degradation (%)	Intensity (W/m ²)	Ref.
TiO ₂	3.2	1.0 g/L (4 hr)	65.67	36.51	59.69	277.92	[40]
ZnO	3.2	1.0 g/L (4 hr)	65.67	36.51	99.64	277.92	[40]
Bi ₂ WO ₆	2.76	1.0 g/L (3 hr)	71.10	29.46	19.6	181.8	[51]
Bi ₂ WO ₆ /NiO	2.62	1.0 g/L (3 hr)	71.10	29.46	48.10	181.8	[51]
Bi ₂ WO ₆ /NiO/Ag	2.35	1.0 g/L (3 hr)	71.10	29.46	88.50	181.8	[51]
SnO ₂	3.7	1.0 g/L (4 hr)	17.59	10.33	79.50	112.53	This Study
SnO ₂	3.7	0.5 g/L (8 hr)	17.59	10.33	91.50	112.53	This Study

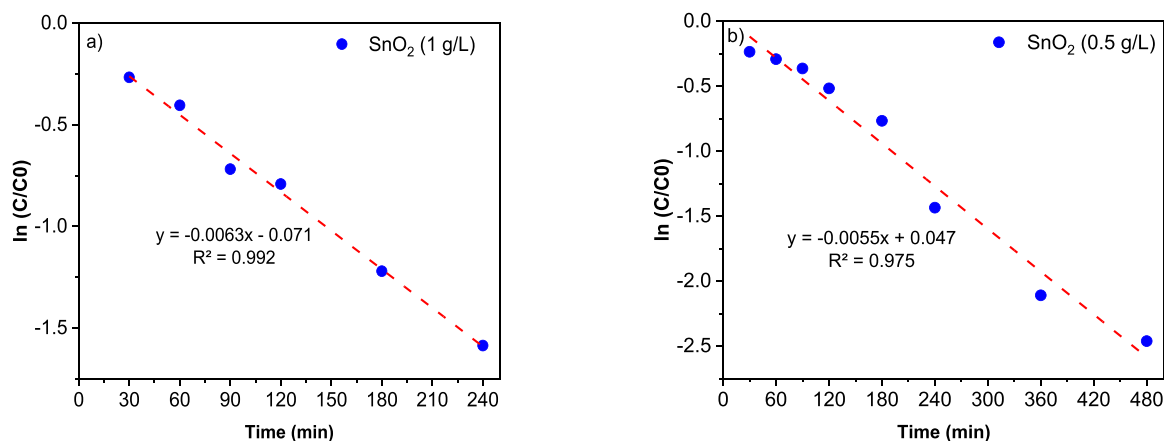


Fig. 4. Pseudo-first-order kinetics of O₂-NAs in the real OSPW; (a) 1.0 g/L and (b) 0.5 g/L of SnO₂. Experimental conditions: dark condition = 60 min; solar irradiance = 112.53 W/m²; pH = 8.32; and treatment time = 8 h.

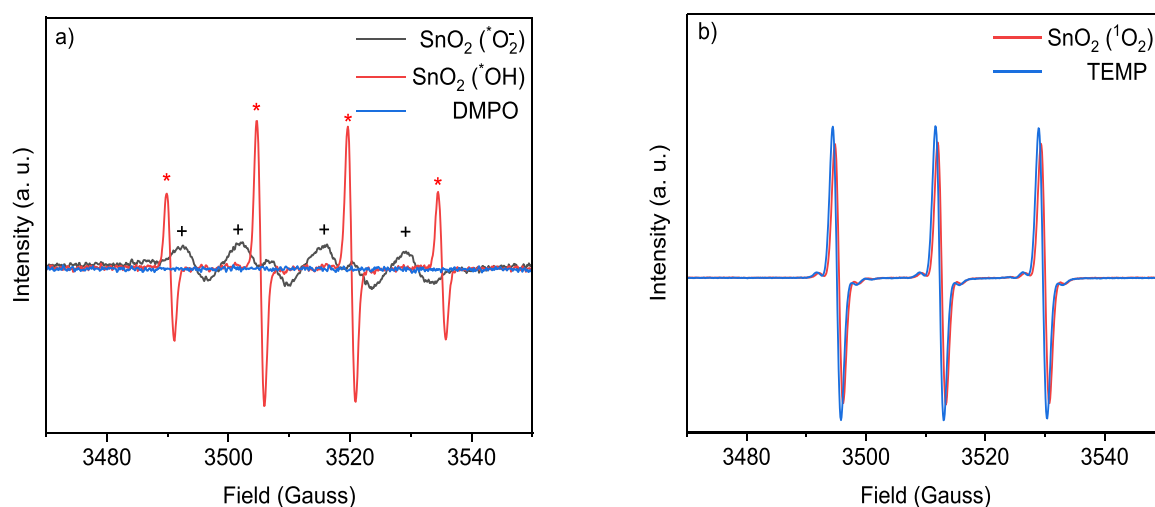


Fig. 5. EPR spectra of the SnO₂ suspensions activated under solar irradiation with the spin trapping agent DMPO and TEMP; a) DMPO•-HO and DMPO•O₂^{•-} adducts; b) TEMP•¹O₂ adduct.

method for assessing HO• radicals. In the present work, spectrophotometric analysis using TA as a target probe was employed to determine the steady-state concentrations of HO• species ([HO•]_{SS}). First, a calibration curve for 2-hydroxyterephthalic acid (hTA), a stable and detectable hydroxylated product of TA [62,69,70], was constructed, as shown in Figure S8. Then, by measuring the reduction in TA concentration due to HO• generation, the [HO•]_{SS} was determined for commonly used commercial photocatalysts and compared to the SnO₂ system, as presented in Fig. 6. This approach can be useful in understanding why certain photocatalysts outperform others in degrading organic contaminants under solar light at similar experimental conditions. The detailed procedure to measure [HO•]_{SS} using TA is provided in Text S4.

The results displayed that the concentration of HO• species followed the order TiO₂ > SnO₂ > WO₃ > CeO₂ > ZnO. However, the literature (Table 1) showed that ZnO exhibits better performance than other photocatalysts, including TiO₂, in degrading classical NAs in OSPW. Based on the results provided by Suara et al. (2022) [40], the difference between ZnO and TiO₂ was mainly attributed to the higher isoelectric points (IEPs) of ZnO ranging from pH 8.0–10.3, compared to IEP values in TiO₂ at an approximate pH of 6.35. While ZnO has an E_g similar to anatase TiO₂ of comparable particle size, its higher IEP makes it less likely to dissolve in a matrix like OSPW (which has a pH above 8). This helps ZnO remain in its solid form, making it readily available for

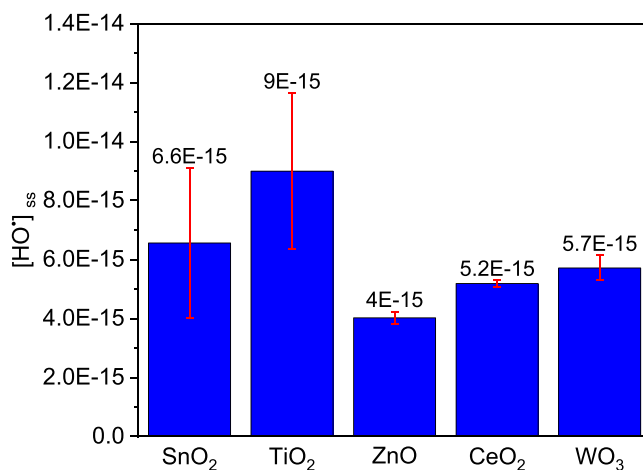


Fig. 6. Estimated HO• concentration at steady-state conditions for commonly used photocatalysts.

photocatalytic activities. Additionally, ZnO particles suspended in real OSPW are likely to exhibit a net positive surface charge (since IEP > pH), potentially boosting the adsorption of negatively charged carboxylates

in real OSPW onto the particles, thereby facilitating oxidation [40]. The higher generation of HO[•] species in SnO₂ compared to most of the studied photocatalysts (WO₃, CeO₂, and ZnO) can be attributed to its higher oxygen vacancies. Despite its wider energy band gap (Eg of 3.6–4.0 eV), the high oxygen vacancies in SnO₂ enhance photocatalytic activity by increasing the availability of reactive sites for electron-hole pair generation and subsequent reactions. Therefore, to address the gap in the degradation of different compounds via photocatalysis, it is important to thoroughly examine the influence of different physico-chemical properties of the photocatalysts, including surface area, particle size, zeta potential, surface charge, IEP, and Eg, as well as the characteristics of the matrix [71,72].

3.7. Efficiency of solar-driven SnO₂ catalysis on the toxicity of real OSPW

The change in acute toxicity was examined to explore the impacts of the breakdown of aromatic mixtures and NAs in real OSPW. The investigation into the acute toxicity of both untreated and treated OSPW involved assessing the inhibitory effects on luminescence in *Vibrio fischeri* (*V. fischeri*) by the Microtox® bioassay, recognized for its expeditious and straightforward assessment of OSPW acute toxicity, has been previously employed in studies [73,74]. As illustrated in Fig. 7, a significant shift in percentage inhibition was observed between untreated OSPW and treated OSPW for both the 5- and 15-minute trials. The outcomes indicated decreases in percentage inhibition from 26.09 % to 7.19 % and 30.85–17.05 % after 5 and 15 min of exposing *V. fischeri* to the treated samples, respectively. Consequently, a substantial reduction in the average acute toxicity of OSPW was achieved, with nearly 92 % catalytic degradation of NAs and aromatic compounds through photocatalysis. These findings underscore the efficacy of the treatment process in concurrently eliminating contaminants and reducing the toxicity of OSPW. The persistent toxicity observed in the treated OSPW could potentially be attributed to organic by-products generated during degradation and non-acidic components inherent to real OSPW. Similar observations of residual toxicity, determined through the Microtox® assay, have been reported in studies employing ozonation, solar-driven catalysis, O₃/H₂O₂ oxidation, and biodegradation for OSPW treatment [40,51,73,75].

As reported in previous studies, alleviating toxic effects in OSPW is intricately linked to the degradation of organic components within the original matrix [48]. Based on Whale et al. [76] work, the toxicology of oily wastewater, as established through standardized bioassays, correlates with the concentration of bioavailable hydrocarbons assessed via BE-SPME [76]. In our investigation, the initial hydrocarbon concentration quantified through BE-SPME analysis (described in Text S5) was

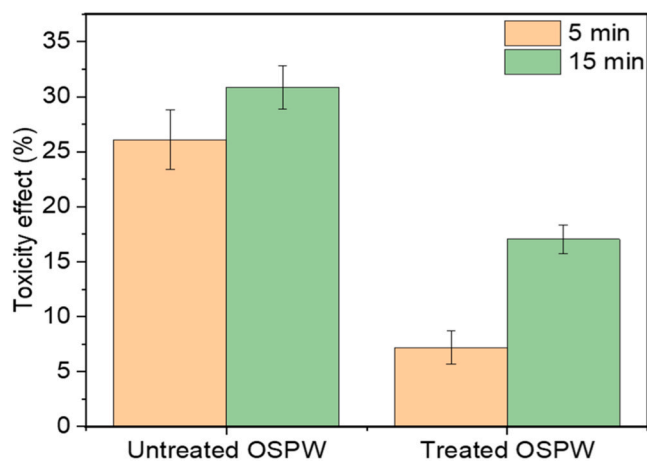


Fig. 7. Microtox® toxicity analysis of untreated and treated real OSPW measured by *Vibrio fischeri*. SnO₂ concentration = 0.5 g/L; dark condition = 60 min; solar irradiance = 112.53 W/m²; pH = 8.32; and treatment time = 8 h.

reduced by approximately 82.0 % after the treatment (Figure S9). Sánchez-Montes et al. (2024) reported an 87 % reduction in bioavailable hydrocarbons from real OSPW using PDS (1 mM) after 60 min of irradiation under UVA LED (0.8 mW/cm²) [48]. In another study, authors demonstrated removing more than 90 % of the bioavailable hydrocarbons of OSPW within a 24-hour adsorption period using activated biochar (2 g/L of SB-Zn) [77]. This efficacy could contribute to the diminished acute toxicity observed in treated OSPW, as measured by the Microtox® bioassay [77].

3.8. Immunotoxic and cytotoxic effects of OSPW after solar-activated SnO₂ photocatalysis

The levels of pro-inflammatory cytokine proteins secreted by mammalian macrophages were measured to explore the immunotoxic effects of raw OSPW compared to OSPW treated with solar-activated SnO₂ photocatalyst. Macrophage cells have previously been used to examine the immunotoxicity of environmental water and wastewater samples [78,79]. In this study, THP-1 and RAW 264.7 cell lines were used. As interleukin-1 beta (IL-1β), interleukin-8 (IL-8), interleukin-6 (IL-6), and tumor necrosis factor-alpha (TNF-α) are key cytokines secreted by macrophage cells in response to environmental toxicants [80,81], their secretion levels were examined as representative inflammatory cytokines following exposures. As demonstrated in Fig. 8, exposure of THP-1 cells to raw OSPW remarkably increased IL-1β and IL-8 secretion compared to the negative control, with levels rising from 0.9 pg/mL to 302.9 pg/mL and 109.94–5087.3 pg/mL, respectively.

Similarly, exposure of RAW 264.7 cells to raw OSPW increased IL-6 and TNF-α secretion levels from 0.33 pg/mL to 4668.1 pg/mL and 23.8–287.1 pg/mL, respectively, after 24 h. Previous research studies have indicated that the organic portions in OSPW mainly contribute to its toxicity [82–84]. However, these fractions have also been shown to possess immunomodulatory properties, possibly inducing inflammatory cytokines in macrophage cells [85]. Therefore, the increased secretion of inflammatory cytokines observed in macrophage cells in our current study could be owing to the presence of the organic constituents within OSPW. Results of our previous studies also support our current study, where we exhibited that secretion levels of these four cytokines were induced when macrophage cells were exposed to untreated OSPW samples for 24 h [48,80].

Notably, solar-activated SnO₂ photocatalytic treatment (at the best condition) of OSPW caused a notable decrease in the levels of all pro-inflammatory cytokines studied. The secretion of IL-1β and IL-8 in THP-1 cells was decreased by 99.5 % and 97.8 %, respectively, whereas levels of IL-6 and TNF-α in RAW 264.7 cells were reduced by 99.9 % and 82.8 %, respectively in treated OSPW. Additionally, the cytokines levels did not meaningfully differ from the secretion values of the negative control. When assessing the four cytokines, the capacity of OSPW to stimulate pro-inflammatory cytokines decreased by nearly 95 % following treatment with solar-activated SnO₂ photocatalysis. This reduction aligns with the targeted components from OSPW, suggesting that solar-activated SnO₂ photocatalysis effectively reduces the immunotoxicity of OSPW, possibly by degrading specific organic constituents such as NAs. Suara et al. (2022) and Paul et al. (2023) reported comparable reductions in these cytokines in both gene and protein expression levels when OSPW samples were treated with solar-activated ZnO photocatalysis [40,80]. Overall, our findings highlight the potential of photocatalytic treatment for reducing the immunotoxic effects of OSPW.

Moreover, the effect of solar-driven SnO₂ catalysis treated and untreated OSPW on the viability of *S. warneri* bacteria was assessed after 22.5 h of exposure. Given that the negative control lacks any compounds that hinder bacterial growth, and all wells received the same concentrations of bacteria and growth medium, the recovery of the negative control is confirmed to be 100 %. As shown in Fig. 9, 22.5 h exposure of *S. warneri* to the untreated OSPW caused a significant decrease in growth compared to the negative control (5.38±0.45 CFU well⁻¹ and 8.02±0.21

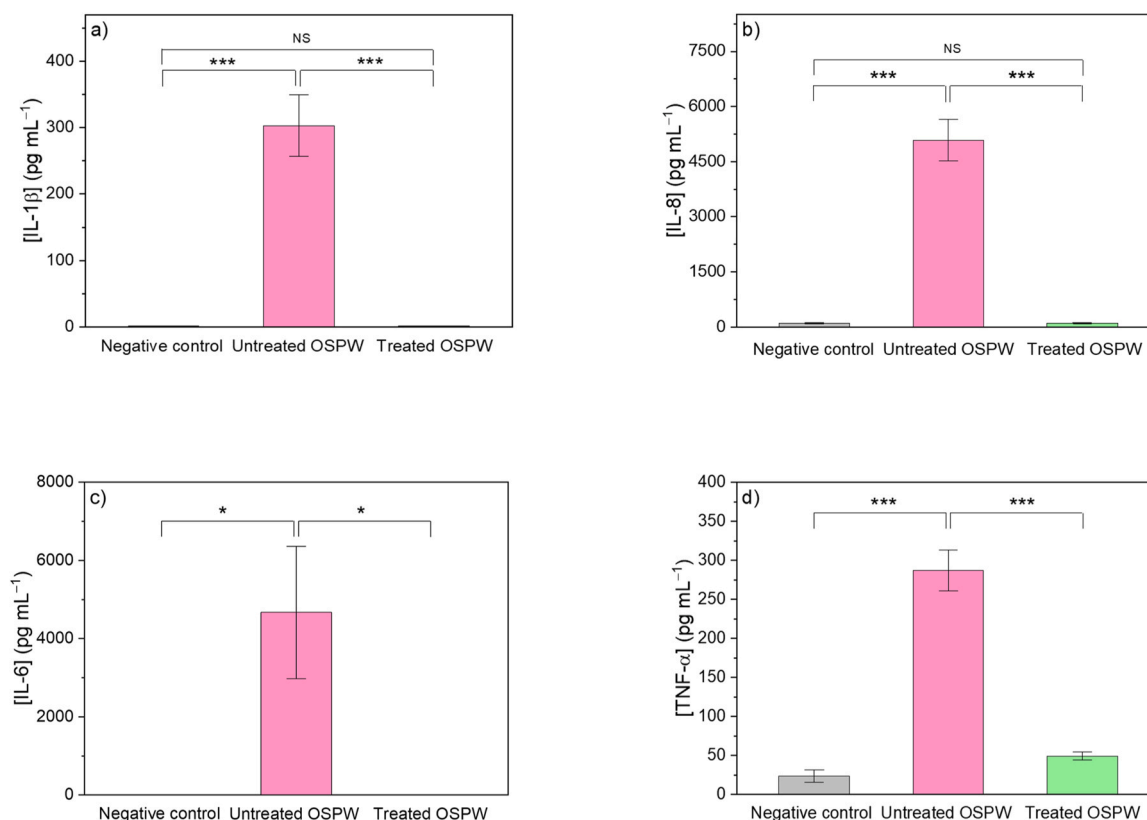


Fig. 8. Secretion levels of pro-inflammatory cytokines following exposure to untreated and treated OSPW samples on macrophage cells. After 24 h of exposure, cytokine secretion levels were analyzed using human and mouse multiplex assays. IL-1 β (a) and IL-8 (b) represent the THP-1 cytokine secretion results, and IL-6 (c) and TNF- α (d) represent the RAW 264.7 cytokine secretion results. Results are denoted as mean \pm SEM for three independent trials ($n=3$). Samples were tested for normal distribution using the Shapiro-Wilk test followed by a One-way ANOVA (Tukey's multiple comparisons) test among the groups. $P < 0.05$ is considered as significant values (***) = $P < 0.001$, ** = $P < 0.002$, * = $P < 0.033$). SnO₂ concentration = 0.5 g/L; dark condition = 60 min; solar irradiance = 112.53 W/m²; pH = 8.32; and treatment time = 8 h.

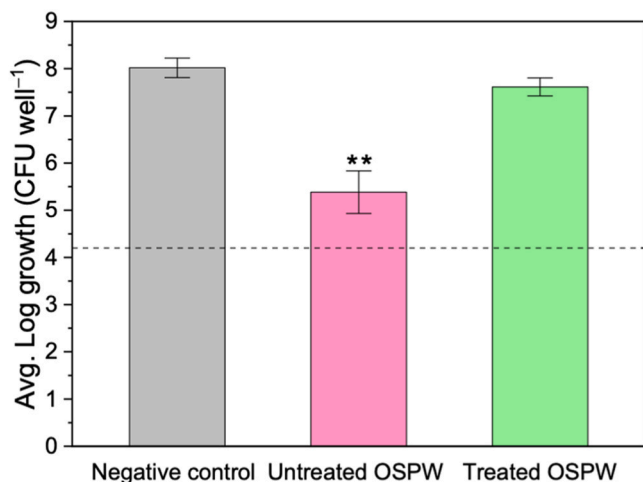


Fig. 9. Average Log growth of *Staphylococcus warneri* after 22.5 h of exposure to untreated and treated OSPW at 35 °C. A solution consisting of ultrapure water with NaCl (1.50 g/L), MgCl₂ (0.35 g/L), and CaCl₂ (0.06 g/L) was utilized as a negative control. Both OSPW samples and the control were diluted at 90 % (V/V) with TSB and inoculated with 6.0 ± 0.5 Log CFU mL⁻¹ of bacteria, resulting in ~ 4.4 Log CFU well⁻¹ of bacteria at time 0 min (indicated by dashed line). After 22.5 h of exposure, samples from each well were serially diluted and spot-platted for enumeration. Significance levels of $P < 0.05$, $P < 0.01$, and $P < 0.001$ are represented by (*), (**), and (***) in the graph, respectively. SnO₂ concentrations = 0.5 g/L; dark condition = 60 min; solar irradiance = 112.53 W/m²; and pH = 8.32.

CFU well⁻¹, respectively). Though still significantly different, the growth of *S. warneri* after exposure to solar-driven SnO₂ catalysis in treated OSPW was close to that observed in the negative control (7.61 ± 0.19 CFU well⁻¹ and 8.02 ± 0.21 CFU well⁻¹, respectively). Growth of *S. warneri* after treatment in treated OSPW was significantly improved compared to the untreated OSPW (7.61 ± 0.19 CFU well⁻¹ and 5.38 ± 0.45 CFU well⁻¹, respectively), with the untreated OSPW seeing a 2.2 Log (158-fold) reduction growth compared to the sample treated with SnO₂ under solar light. This significant improvement in bacterial viability suggests that the treatment of the OSPW via 0.5 g/L of SnO₂ after 8 h of exposure to simulated solar light reduces the presence of constituents that negatively affect bacterial growth. An alternative visualization of this data is presented in Figure S9, illustrating a remarkable decrease in average Log reduction of *S. warneri* viability after treatment compared to untreated OSPW Figure S10.

3.9. Leaching test

The potential leaching of metals from metal oxide or metal sulfide photocatalysts, when applied in water and wastewater treatment, raises concerns about their applications. Thus, a leaching test was performed to assess the potential release of Sn from the photocatalysts into the solution during the treatment process, using inductively coupled plasma optical emission spectrometry (ICP-OES, Thermo iCAP6300 Duo). Solar-driven catalysis experiments were conducted with different concentrations of SnO₂ under solar light irradiation for 4, 8, and 24 h. The Sn concentrations in untreated and SnO₂-treated OSPW were measured and presented in Table S3. Sn in all samples was below 0.002 mg/L, corresponding to the detection limit of the equipment. Notably, no specific

permissible limit is established for Sn in drinking water quality guidelines. However, with a detected concentration of 0.002 mg/L, lower than the permissible limits set for the most toxic metals, this underscores the favorable outcome for the application of SnO₂ photocatalyst in treating OSPW in real-world scenarios.

3.10. Potential application of solar-driven SnO₂ catalysis in NAs removal from tailing ponds

The management of tailings ponds poses an environmental challenge. Currently, these ponds occupy a considerable area in Alberta, spanning approximately 77 km². Solar-driven AOPs represent a promising solution with the potential to degrade complex and toxic compounds, including NAs [86]. According to Environment Canada data from 1981 to 2010, the average percentage of sunlight hours, termed % Sun, stands at 52 % and 50 % for the Alberta cities Calgary and Edmonton, respectively. Additionally, the average annual hours of bright sunshine were reported as 2396 for Calgary and 2345 for Edmonton [87]. In this sense, to assess the SnO₂ performance under conditions mimicking those typical of several months in Alberta, long-term experiments involving up to 24 h of irradiation. Due to technical limitations, these experiments were conducted for 8 h per day over 3 consecutive days. To prevent any additional degradation from environmental light sources, samples were properly covered and stored when not exposed to solar light. The results, illustrated in Fig. 10, confirmed the excellent performance of SnO₂ under solar light, with approximately 90 % degradation observed for both doses (0.1 and 0.5 g/L) after 24 and 16 h, respectively. Despite these promising results, parameters associated with the costs of the SnO₂, as well as other operational expenses, need to be considered in future studies for practical applications.

4. Conclusions

The efficiency of SnO₂ under solar light to degrade NAs and FOCs in real OSPW was successfully investigated. Over 91 % of classical NAs in the matrix were degraded using 0.5 g/L of SnO₂ after 8 h of irradiation. HO[•] and O₂^{•-} species played a crucial role in the degradation of NAs and the degradation of another organic contaminant in OSPW. Structural dependence in NAs degradation was observed, influenced by DBE and carbon content. The process revealed high selectivity, preferentially removing fluorescing aromatics with two rings and three rings and NAs with high carbon and DBE values, representing the most environmentally persistent portions of NAs. The performance of the system was also evaluated for its impact on decreasing the toxicity of real OSPW. Acute toxicity of treated OSPW significantly decreased, and around 82.0 % reduction was observed in the concentration of bioavailable hydrocarbons. Furthermore, THP-1 macrophage cells secrete significantly lower concentrations of proinflammatory biomarkers when exposed to treated OSPW by SnO₂ under solar light compared to untreated OSPW, and remaining organic fractions do not markedly affect the viability of *S. warneri*. In this sense, solar-driven SnO₂ catalysis is a robust and efficient method for treating real OSPW and reducing its pre-existing toxicity. These insights provide valuable guidance for advancing sustainable approaches to OSPW treatment within a concise framework.

CRedit authorship contribution statement

Hadi Mokarizadeh: Writing – review & editing, Writing – original draft, Visualization, Methodology, Conceptualization. **Isaac Sánchez-Montes:** Writing – review & editing, Conceptualization. **Sunanda Paul:** Writing – review & editing, Formal analysis. **Nora A. S. Hussain:** Writing – review & editing, Formal analysis. **Kareem Moghrabi:** Writing – review & editing, Formal analysis. **James L. Stafford:** Writing – review & editing, Formal analysis. **Mohamed Gamal El-Din:** Writing – review & editing, Supervision, Project administration, Funding

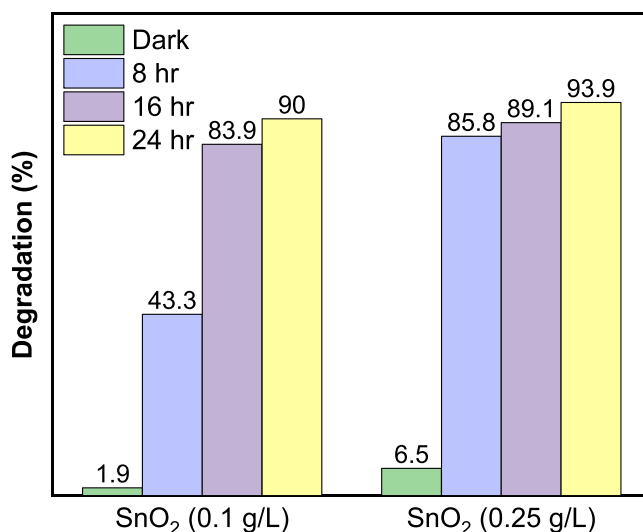


Fig. 10. Effect of SnO₂ photocatalyst under dark conditions and solar light on the degradation of O₂-NAs in real OSPW. Experimental conditions: SnO₂ concentrations = 0.1, and 0.25 g/L; dark condition = 60 min; solar irradiance = 112.53 W/m²; and pH = 8.32.

acquisition.

Declaration of Competing Interest

The authors declare the following financial interests/personal relationships which may be considered as potential competing interests: Mohamed Gamal El-Din reports financial support was provided by Natural Sciences and Engineering Research Council of Canada. Mohamed Gamal El-Din reports financial support was provided by Canada's Oil Sands Innovation Alliance. Mohamed Gamal El-Din reports financial support was provided by Suncor Energy Inc. Mohamed Gamal El-Din reports financial support was provided by Syncrude Canada Ltd. Mohamed Gamal El-Din reports financial support was provided by Imperial Oil Resources Ltd. Mohamed Gamal El-Din reports financial support was provided by Teck Resources Limited. Mohamed Gamal El-Din reports financial support was provided by Canadian Natural Resources Limited. Mohamed Gamal El-Din reports financial support was provided by Alberta Innovates. Mohamed Gamal El-Din reports financial support was provided by EPCOR Water Services Inc. Mohamed Gamal El-Din reports financial support was provided by Alberta Environment and Parks. Mohamed Gamal El-Din reports financial support was provided by Canada First Research Excellence Fund. If there are other authors, they declare that they have no known competing financial interests or personal relationships that could have appeared to influence the work reported in this paper.

Data availability

No data was used for the research described in the article.

Acknowledgments

This study was supported by a research grant from the Natural Sciences and Engineering Research Council of Canada (NSERC) Senior Industrial Research Chair (IRC) in Oil Sands Tailings Water Treatment, with the backing of Canada's Oil Sands Innovation Alliance (COSIA), Syncrude Canada Ltd., Suncor Energy Inc., Imperial Oil Resources Ltd., Teck Resources Limited, Canadian Natural Resources Limited, Alberta Innovates, EPCOR Water Services Inc., and Alberta Environment and Parks. This research is also supported by the University of Alberta's Future Energy Systems research initiative, supported by the Canada First

Research Excellence Fund. The authors acknowledge Dr. Pamela Chelme-Ayala for her assistance in conceptualizing and discussing this study.

Appendix A. Supporting information

Supplementary data associated with this article can be found in the online version at [doi:10.1016/j.jece.2024.114168](https://doi.org/10.1016/j.jece.2024.114168).

References

- [1] S.A. Messele, P. Chelme-Ayala, M. Gamal El-Din, Catalytic ozonation of naphthenic acids in the presence of carbon-based metal-free catalysts: performance and kinetic study, *Catal. Today* 361 (2021) 102–108, <https://doi.org/10.1016/J.CATTOD.2020.01.042>.
- [2] R. Qin, D. Lillico, Z.T. How, R. Huang, M. Belosevic, J. Stafford, M. Gamal El-Din, Separation of oil sands process water organics and inorganics and examination of their acute toxicity using standard in-vitro bioassays, *Sci. Total Environ.* 695 (2019) 133532, <https://doi.org/10.1016/J.SCITOTENV.2019.07.338>.
- [3] Y. Ju, C. Liu, S.O. Ganiyu, Y. Zhao, M. Gamal El-Din, Electrochemical degradation of dissolved organic matters in oil sands process water using continuous-flow packed bed electrode reactor, *Sep. Purif. Technol.* 320 (2023) 124135, <https://doi.org/10.1016/J.SEPPUR.2023.124135>.
- [4] H. Mokarizadeh, A. Raisi, Industrial wastewater treatment using PES UF membranes containing hydrophilic additives: experimental and modeling of fouling mechanism, *Environ. Technol. Innov.* 23 (2021) 101701, <https://doi.org/10.1016/J.ETI.2021.101701>.
- [5] R. Huang, Y. Chen, M.N.A. Meshref, P. Chelme-Ayala, S. Dong, M.D. Ibrahim, C. Wang, N. Klammerth, S.A. Hughes, J.V. Headley, K.M. Peru, C. Brown, A. Mahaffey, M. Gamal El-Din, Characterization and determination of naphthenic acids species in oil sands process-affected water and groundwater from oil sands development area of Alberta, Canada, *Water Res* 128 (2018) 129–137, <https://doi.org/10.1016/J.WATRES.2017.10.003>.
- [6] A. Mahaffey, M. Dubé, Review of the composition and toxicity of oil sands process-affected water, *Environ. Rev.* 25 (2017) 97–114, https://doi.org/10.1139/ER-2015-0060/SUPPL_FILE/ER-2015-0060SUPPL.PDF.
- [7] N.A.S. Hussain, J.L. Stafford, Abiotic and biotic constituents of oil sands process-affected waters, *J. Environ. Sci.* 127 (2023) 169–186, <https://doi.org/10.1016/J.JES.2022.06.012>.
- [8] E.K. Quagraine, H.G. Peterson, J.V. Headley, In situ bioremediation of naphthenic acids contaminated tailing pond waters in the athabasca oil sands region—demonstrated field studies and plausible options: a review, *J. Environ. Sci. Heal.* 40 (2005) 685–722, <https://doi.org/10.1081/ESE-200046649>.
- [9] A.E. Bauer, L.M. Hewitt, J.L. Parrott, A.J. Bartlett, P.L. Gillis, L.E. Deeth, M. D. Rudy, R. Vanderveen, L. Brown, S.D. Campbell, M.R. Rodrigues, A.J. Farwell, D. G. Dixon, R.A. Frank, The toxicity of organic fractions from aged oil sands process-affected water to aquatic species, *Sci. Total Environ.* 669 (2019) 702–710, <https://doi.org/10.1016/J.SCITOTENV.2019.03.107>.
- [10] A.C. Scott, W. Zubot, C.W. Davis, J. Brogly, Bioaccumulation potential of naphthenic acids and other ionizable dissolved organics in oil sands process water (OSPW) – A review, *Sci. Total Environ.* 712 (2020) 134558, <https://doi.org/10.1016/J.SCITOTENV.2019.134558>.
- [11] C. Li, L. Fu, J. Stafford, M. Belosevic, M. Gamal El-Din, The toxicity of oil sands process-affected water (OSPW): a critical review, *Sci. Total Environ.* 601–602 (2017) 1785–1802, <https://doi.org/10.1016/J.SCITOTENV.2017.06.024>.
- [12] H. Jia, G. xi Zhang, Y. fan Wu, W. wei Dai, Q. bin Xu, S. Gan, X. yun Ju, Z. zhong Feng, R. peng Li, B. Yuans, Evaluation of negative effect of Naphthenic acids (NAs) on physiological metabolism and polycyclic aromatic hydrocarbons adsorption of *Phragmites australis*, *Chemosphere* 318 (2023) 137909, <https://doi.org/10.1016/J.CHEMOSPHERE.2023.137909>.
- [13] X. Han, M.D. MacKinnon, J.W. Martin, Estimating the in situ biodegradation of naphthenic acids in oil sands process waters by HPLC/HRMS, *Chemosphere* 76 (2009) 63–70, <https://doi.org/10.1016/J.CHEMOSPHERE.2009.02.026>.
- [14] E.K. Quagraine, H.G. Peterson, J.V. Headley, In situ bioremediation of naphthenic acids contaminated tailing pond waters in the Athabasca oil sands region - Demonstrated field studies and plausible options: a review, *J. Environ. Sci. Heal. - Part A Toxic. /Hazard. Subst. Environ. Eng.* 40 (2005) 685–722, <https://doi.org/10.1081/ESE-200046649>.
- [15] X. Han, M.D. MacKinnon, J.W. Martin, Estimating the in situ biodegradation of naphthenic acids in oil sands process waters by HPLC/HRMS, *Chemosphere* 76 (2009) 63–70, <https://doi.org/10.1016/j.chemosphere.2009.02.026>.
- [16] T.M. Misiti, U. Tezel, S.G. Pavlostathis, Effect of alkyl side chain location and cyclicity on the aerobic biotransformation of naphthenic acids, *Environ. Sci. Technol.* 48 (2014) 7909–7917, https://doi.org/10.1021/ES501058Q/SUPPL_FILE/ES501058Q_SI_001.PDF.
- [17] T. Dong, Y. Zhang, M.S. Islam, Y. Liu, M. Gamal El-Din, The impact of various ozone pretreatment doses on the performance of endogenous microbial communities for the remediation of oil sands process-affected water, *Int. Biodeterior. Biodegrad.* 100 (2015) 17–28, <https://doi.org/10.1016/J.IBIOD.2015.01.014>.
- [18] M. Gamal El-Din, H. Fu, N. Wang, P. Chelme-Ayala, L. Pérez-Estrada, P. Drzewicz, J.W. Martin, W. Zubot, D.W. Smith, Naphthenic acids speciation and removal during petroleum-coke adsorption and ozonation of oil sands process-affected water, *Sci. Total Environ.* 409 (2011) 5119–5125, <https://doi.org/10.1016/J.SCITOTENV.2011.08.033>.
- [19] Z. Fang, P. Chelme-Ayala, Q. Shi, C. Xu, M. Gamal El-Din, Degradation of naphthenic acid model compounds in aqueous solution by UV activated persulfate: Influencing factors, kinetics and reaction mechanisms, *Chemosphere* 211 (2018) 271–277, <https://doi.org/10.1016/J.CHEMOSPHERE.2018.07.132>.
- [20] A. Afzal, P. Chelme-Ayala, P. Drzewicz, J.W. Martin, M. Gamal El-Din, Effects of Ozone and Ozone/Hydrogen Peroxide on the Degradation of Model and Real Oil-Sands-Process-Affected-Water Naphthenic Acids, *Ozone Sci. Eng.* 37 (2015) 45–54, <https://doi.org/10.1080/01919512.2014.967835>.
- [21] S.O. Ganiyu, M. Gamal El-Din, Insight into in-situ radical and non-radical oxidative degradation of organic compounds in complex real matrix during electrooxidation with boron doped diamond electrode: a case study of oil sands process water treatment, *Appl. Catal. B Environ.* 279 (2020) 119366, <https://doi.org/10.1016/J.APCATB.2020.119366>.
- [22] A.S. Abdalrhman, M. Gamal El-Din, Degradation of organics in real oil sands process water by electro-oxidation using graphite and dimensionally stable anodes, *Chem. Eng. J.* 389 (2020) 124406, <https://doi.org/10.1016/J.CEJ.2020.124406>.
- [23] Y. Zhang, N. Klammerth, P. Chelme-Ayala, M. Gamal El-Din, Comparison of classical fenton, nitritotriacetic acid (NTA)-Fenton, UV-Fenton, UV photolysis of Fe-NTA, UV-NTA-Fenton, and UV-H2O2 for the degradation of cyclohexanoic acid, *Chemosphere* 175 (2017) 178–185, <https://doi.org/10.1016/J.CHEMOSPHERE.2017.02.058>.
- [24] P.V. Nidheesh, G. Divyapriya, F. Ezzahra Titchou, M. Hamdani, Treatment of textile wastewater by sulfate radical based advanced oxidation processes, *Sep. Purif. Technol.* 293 (2022) 121115, <https://doi.org/10.1016/J.SEPPUR.2022.121115>.
- [25] J.A. Garrido-Cardenas, B. Esteban-García, A. Agüera, J.A. Sánchez-Pérez, F. Manzano-Agugliaro, Wastewater treatment by advanced oxidation process and their worldwide research trends, *Page 170, Int. J. Environ. Res. Public Heal.* 2020 Vol. 17 (17) (2019) 170, <https://doi.org/10.3390/IJERPH17010170>.
- [26] Z. Shu, J.R. Bolton, M. Belosevic, M. Gamal El Din, Photodegradation of emerging micropollutants using the medium-pressure UV/H2O2 Advanced Oxidation Process, *Water Res* 47 (2013) 2881–2889, <https://doi.org/10.1016/J.WATRES.2013.02.045>.
- [27] U.I. Gaya, A.H. Abdullah, Heterogeneous photocatalytic degradation of organic contaminants over titanium dioxide: a review of fundamentals, progress and problems, *J. Photochem. Photobiol. C. Photochem. Rev.* 9 (2008) 1–12, <https://doi.org/10.1016/J.JPHOTOCHEMREV.2007.12.003>.
- [28] L. Spadaro, F. Arena, A. Palella, Which Future Route in the Methanol Synthesis? Photocatalytic Reduction of CO2, the new challenge in the solar energy exploitation, *Methanol Sci. Eng.* (2018) 429–472, <https://doi.org/10.1016/B978-0-444-63903-5.00016-9>.
- [29] H. Zhang, G. Zhao, T. Zhang, F. Teng, Syntheses and photocatalytic performances of vertically grown Fe2O3 and TiO2/Fe2O3 nanorods on coated glass substrates, *J. Alloy. Compd.* 603 (2014) 35–41, <https://doi.org/10.1016/J.JALLCOM.2014.03.042>.
- [30] M.R. Al-Mamun, S. Kader, M.S. Islam, M.Z.H. Khan, Photocatalytic activity improvement and application of UV-TiO2 photocatalysis in textile wastewater treatment: a review, *J. Environ. Chem. Eng.* 7 (2019) 103248, <https://doi.org/10.1016/J.JECE.2019.103248>.
- [31] Z. Li, Z. Li, C. Zuo, X. Fang, Z.L. Li, Z.Q. Li, C.L. Zuo, X.S. Fang, Application of nanostructured TiO2 in UV photodetectors: a review, *Adv. Mater.* 34 (2022) 2109083, <https://doi.org/10.1002/ADMA.202109083>.
- [32] D.R. Rosaline, A. Suganthi, G. Vinodhkumar, S.S.R. Inbanathan, A. Umar, S. Ameen, M.S. Akhtar, E. LuizFoletto, Enhanced sunlight-driven photocatalytic activity of SnO2-Sb2O3 composite towards emerging contaminant degradation in water, *J. Alloy. Compd.* 897 (2022) 162935, <https://doi.org/10.1016/J.JALLCOM.2021.162935>.
- [33] G.K. Dalapati, H. Sharma, A. Guchhait, N. Chakraborty, P. Bamola, Q. Liu, G. Saianand, A.M. Sai Krishna, S. Mukhopadhyay, A. Dey, T.K.S. Wong, S. Zhuk, S. Ghosh, S. Chakraborty, C. Mahata, S. Biring, A. Kumar, C.S. Ribeiro, S. Ramakrishna, A.K. Chakraborty, S. Krishnamurthy, P. Sonar, M. Sharma, Tin oxide for optoelectronic, photovoltaic and energy storage devices: a review, *J. Mater. Chem. A* 9 (2021) 16621–16684, <https://doi.org/10.1039/D1TA01291F>.
- [34] S.J. Keny, A.P. Srivastava, A.K. Debnath, S. Adhikari, M.C. Rath, One-step synthesis of tin oxide nanoparticles in aqueous solution induced by free radicals, *Mater. Chem. Phys.* 286 (2022) 126184, <https://doi.org/10.1016/J.MATCHEMPHYS.2022.126184>.
- [35] C. Zeng, L.S. Tsui, F.L.Y. Lam, T. Wu, A.C.K. Yip, Revisiting the crucial roles of oxygen vacancies in photo/electro-catalytic degradation of aqueous organic pollutants, *Appl. Catal. O Open.* 190 (2024) 206930, <https://doi.org/10.1016/J.APCATO.2024.206930>.
- [36] J. Lincho, E. Domingues, P. Mazierski, M. Miodyńska, T. Klimczuk, A. Zaleska-Medynska, R.C. Martins, J. Gomes, The role of noble metals in TiO2 nanotubes for the abatement of parabens by photocatalysis, catalytic and photocatalytic ozonation, *Sep. Purif. Technol.* 326 (2023) 124747, <https://doi.org/10.1016/J.SEPPUR.2023.124747>.
- [37] J. Xu, P. Liang, X. Shen, F. Wang, Y. Lou, J. Zhang, C. Pan, Y. Zhu, Z. Wang, High-efficiency removal of organic pollutants, antibiotic resistant bacteria and resistance genes by a photocatalysis-self-Fenton system based on S, K co-doped g-C3N4 nanosheets, *Sep. Purif. Technol.* 339 (2024) 126734, <https://doi.org/10.1016/J.SEPPUR.2024.126734>.
- [38] T. Zhang, E. Shang, Z. Liao, Z. Xu, J. Luo, C. Wang, C. Ni, J.P. Ni, Simulated solar-driven photo-assisted anodic oxidation of sulfadiazine by C3N4 modified Ti3+ self-

- doping TiO₂ nanotube arrays, Sep. Purif. Technol. 334 (2024) 126055, <https://doi.org/10.1016/J.SEPPUR.2023.126055>.
- [39] S. Sunuwar, C.E. Manzanares, Excitation, emission, and synchronous fluorescence for astrochemical applications: experiments and computer simulations of synchronous spectra of polycyclic aromatic hydrocarbons and their mixtures, Icarus 370 (2021) 114689, <https://doi.org/10.1016/J.ICARUS.2021.114689>.
- [40] M.A. Suares, S.O. Ganiyu, S. Paul, J.L. Stafford, M. Gamal El-Din, Solar-activated zinc oxide photocatalytic treatment of real oil sands process water: effect of treatment parameters on naphthenic acids, polyaromatic hydrocarbons and acute toxicity removal, Sci. Total Environ. 819 (2022) 153029, <https://doi.org/10.1016/J.SCITOTENV.2022.153029>.
- [41] Z. Fang, R. Huang, P. Chelme-Ayala, Q. Shi, C. Xu, M. Gamal El-Din, Comparison of UV/Persulfate and UV/H₂O₂ for the removal of naphthenic acids and acute toxicity towards *Vibrio fischeri* from petroleum production process water, Sci. Total Environ. 694 (2019) 133686, <https://doi.org/10.1016/J.SCITOTENV.2019.133686>.
- [42] R. Qin, Z.T. How, M. Gamal El-Din, Photodegradation of naphthenic acids induced by natural photosensitizer in oil sands process water, Water Res 164 (2019) 114913, <https://doi.org/10.1016/J.WATRES.2019.114913>.
- [43] C. Wang, N. Klammerth, S.A. Messele, A. Singh, M. Belosevic, M. Gamal El-Din, Comparison of UV/hydrogen peroxide, potassium ferrate(VI), and ozone in oxidizing the organic fraction of oil sands process-affected water (OSPW), Water Res 100 (2016) 476–485, <https://doi.org/10.1016/J.WATRES.2016.05.037>.
- [44] S.O. Ganiyu, C.A. Martínez-Huitle, Nature, mechanisms and reactivity of electrogenerated reactive species at thin-film boron-doped diamond (bdd) electrodes during electrochemical wastewater treatment, ChemElectroChem 6 (2019) 2379–2392, <https://doi.org/10.1002/CELC.201900159>.
- [45] C. von Sonntag, U. von Gunten, Chemistry of Ozone in Water and Wastewater Treatment, Chem. Ozone Water Wastewater Treat. From Basic Principles to Appl. (2012) 225–248. (<https://iwaponline.com/ebooks/book-pdf/650791/wio9781780400839.pdf>) (accessed January 30, 2024).
- [46] T. Leshuk, T. Wong, S. Linley, K.M. Peru, J.V. Headley, F. GuSolar photocatalytic degradation of naphthenic acids in oil sands process-affected water 144 Chemosphere, 2016, 1854–1861, 10.1016/J.CHEMOSPHERE.2015.10.073.
- [47] X. Liang, X. Zhu, E.C. Butler, Comparison of four advanced oxidation processes for the removal of naphthenic acids from model oil sands process water, J. Hazard. Mater. 190 (2011) 168–176, <https://doi.org/10.1016/J.JHAZMAT.2011.03.022>.
- [48] I. Sánchez-Montes, H. Mokarizadeh, S. Paul, K. Moghrabi, N. Hussain, P. Chelme-Ayala, J.L. Stafford, M.R.V. Lanza, M. Gamal El-Din, U.V.A. LED-assisted, breakdown of persulfate oxidants for the treatment of real oil sands process water: removal of naphthenic acids and evaluation of residual toxicity, Chem. Eng. J. 481 (2024) 148631, <https://doi.org/10.1016/J.CEJ.2024.148631>.
- [49] N. Klammerth, J. Moreira, C. Li, A. Singh, K.N. McPhedran, P. Chelme-Ayala, M. Belosevic, M. Gamal El-Din, Effect of ozonation on the naphthenic acids' speciation and toxicity of pH-dependent organic extracts of oil sands process-affected water, Sci. Total Environ. 506–507 (2015) 66–75, <https://doi.org/10.1016/J.SCITOTENV.2014.10.103>.
- [50] M.N.A. Meshref, N. Klammerth, M.S. Islam, K.N. McPhedran, M. Gamal El-Din, Understanding the similarities and differences between ozone and peroxone in the degradation of naphthenic acids: comparative performance for potential treatment, Chemosphere 180 (2017) 149–159, <https://doi.org/10.1016/J.CHEMOSPHERE.2017.03.113>.
- [51] L. Meng, Z.T. How, P. Chelme-Ayala, C. Benally, M. Gamal El-Din, Z-scheme plasmonic Ag decorated Bi₂WO₆/NiO hybrids for enhanced photocatalytic treatment of naphthenic acids in real oil sands process water under simulated solar irradiation, J. Hazard. Mater. 454 (2023) 131441, <https://doi.org/10.1016/J.JHAZMAT.2023.131441>.
- [52] S. Yue, B.A. Ramsay, J. Wang, J. Ramsay, Toxicity and composition profiles of solid phase extracts of oil sands process-affected water, Sci. Total Environ. 538 (2015) 573–582, <https://doi.org/10.1016/J.SCITOTENV.2015.08.079>.
- [53] K.E. Tollefsen, K. Petersen, S.J. Rowland, Toxicity of synthetic naphthenic acids and mixtures of these to fish liver cells, Environ. Sci. Technol. 46 (2012) 5143–5150, https://doi.org/10.1021/ES204124W/SUPPL_FILE/ES204124W_SI_001.PDF.
- [54] H.C. Reinardy, A.G. Scarlett, T.B. Henry, C.E. West, L.M. Hewitt, R.A. Frank, S. J. Rowland, Aromatic naphthenic acids in oil sands process-affected water, resolved by GCxGC-MS, only weakly induce the gene for vitellogenin production in zebrafish (*Danio rerio*) larvae, Environ. Sci. Technol. 47 (2013) 6614–6620, https://doi.org/10.1021/ES304799M/SUPPL_FILE/ES304799M_SI_001.PDF.
- [55] A. Afzal, P. Drzewicz, J.W. Martin, M. Gamal El-Din, Decomposition of cyclohexanoic acid by the UV/H₂O₂ process under various conditions, Sci. Total Environ. 426 (2012) 387–392, <https://doi.org/10.1016/J.SCITOTENV.2012.03.019>.
- [56] K. Reszka, P. Bilski, C.F. Chignell, EPR spectra of DMPO spin adducts of superoxide and hydroxyl radicals in pyridine, Free Radic. Res. Commun. 17 (1992) 377–385, <https://doi.org/10.3109/10715769209083142>.
- [57] S.K. Han, T.M. Hwang, Y. Yoon, J.W. Kang, Evidence of singlet oxygen and hydroxyl radical formation in aqueous goethite suspension using spin-trapping electron paramagnetic resonance (EPR), Chemosphere 84 (2011) 1095–1101, <https://doi.org/10.1016/J.CHEMOSPHERE.2011.04.051>.
- [58] T. Shi, R.P.F. Schins, A.M. Knaapen, T. Kuhlbusch, M. Pitz, J. Heinrich, P.J. A. Borm, Hydroxyl radical generation by electron paramagnetic resonance as a new method to monitor ambient particulate matter composition, J. Environ. Monit. 5 (2003) 550–556, <https://doi.org/10.1039/B303928P>.
- [59] H.F.V. Victória, D.C. Ferreira, J.B.G. Filho, D.C.S. Martins, M.V.B. Pinheiro, G.A. M. Safa, K. Krambrock, Detection of singlet oxygen by EPR: the instability of the nitroxyl radicals, Free Radic. Biol. Med. 180 (2022) 143–152, <https://doi.org/10.1016/J.FREERADBIOMED.2021.12.303>.
- [60] G. Nardi, I. Manet, S. Monti, M.A. Miranda, V. Lhiaubet-Vallet, Scope and limitations of the TEMPO/EPR method for singlet oxygen detection: the misleading role of electron transfer, Free Radic. Biol. Med. 77 (2014) 64–70, <https://doi.org/10.1016/J.FREERADBIOMED.2014.08.020>.
- [61] S. Wei, J. Liu, Y. Zhao, T. Zhang, M. Zheng, F. Jin, X. Dong, J. Xing, X. Duan, Protein-Based 3D Microstructures with Controllable Morphology and pH-Responsive Properties, ACS Appl. Mater. Interfaces 9 (2017) 42247–42257, https://doi.org/10.1021/ACSAMI.7B14915/ASSET/IMAGES/LARGE/AM-2017-14915T_0010.JPEG.
- [62] S.J. De-Nasri, S. Nagarajan, P.K.J. Robertson, V.V. Ranade, Quantification of hydroxyl radicals in photocatalysis and acoustic cavitation: utility of coumarin as a chemical probe, Chem. Eng. J. 420 (2021) 127560, <https://doi.org/10.1016/J.CEJ.2020.127560>.
- [63] M.G. Steiner, C.F. Babbs, Quantitation of the hydroxyl radical by reaction with dimethyl sulfoxide, Arch. Biochem. Biophys. 278 (1990) 478–481, [https://doi.org/10.1016/0003-9861\(90\)90288-A](https://doi.org/10.1016/0003-9861(90)90288-A).
- [64] R.S. Lankone, A.R. Deline, M. Barclay, D.H. Fairbrother, UV-Vis quantification of hydroxyl radical concentration and dose using principal component analysis, Talanta 218 (2020) 121148, <https://doi.org/10.1016/J.TALANTA.2020.121148>.
- [65] E.G. Janzen, Y. Kotake, H. Randall, D. Stabilities, of hydroxyl radical spin adducts of PBN-type spin traps, Free Radic. Biol. Med. 12 (1992) 169–173, [https://doi.org/10.1016/0891-5849\(92\)90011-5](https://doi.org/10.1016/0891-5849(92)90011-5).
- [66] P. Šunka, V. Babický, M. Člupek, P. Lukeš, M. Šimek, J. Schmidt, M. Černák, Generation of chemically active species by electrical discharges in water, Plasma Sources Sci. Technol. 8 (1999) 258, <https://doi.org/10.1088/0963-0252/8/2/006>.
- [67] M. Sahni, B.R. Locke, Quantification of hydroxyl radicals produced in aqueous phase pulsed electrical discharge reactors, Ind. Eng. Chem. Res. 45 (2006) 5819–5825, <https://doi.org/10.1021/IE0601504/ASSET/IMAGES/LARGE/IE0601504F00008.JPEG>.
- [68] Q. Xiang, J. Yu, P.K. Wong, Quantitative characterization of hydroxyl radicals produced by various photocatalysts, J. Colloid Interface Sci. 357 (2011) 163–167, <https://doi.org/10.1016/J.JCIS.2011.01.093>.
- [69] B. Aoudi, J. Kahkeci, Y. Boluk, M. Gamal El-Din, Enhanced g-C₃N₄ for sustainable solar degradation of 1,3-diphenylguanidine (DPG) in wastewater: investigating the effects of precursor, temperature, and potassium doping, Chem. Eng. J. 487 (2024) 150665, <https://doi.org/10.1016/J.CEJ.2024.150665>.
- [70] T. Zeng, W.A. Arnold, Pesticide photolysis in prairie potholes: Probing photosensitized processes, Environ. Sci. Technol. 47 (2013) 6735–6745, https://doi.org/10.1021/ES3030808/SUPPL_FILE/ES3030808_SI_001.PDF.
- [71] C.S. Cao, J. Wang, L. Yang, J. Wang, Y. Zhang, L. Zhu, A review on the advancement in photocatalytic degradation of poly/perfluoroalkyl substances in water: Insights into the mechanisms and structure-function relationship, Sci. Total Environ. 946 (2024) 174137, <https://doi.org/10.1016/J.SCITOTENV.2024.174137>.
- [72] G. Singh, M.K. Ubhi, K. Jeet, C. Singla, M. Kaur, A review on impacting parameters for photocatalytic degradation of organic effluents by ferrites and their nanocomposites, Page 1727, Process 2023 Vol. 11 (11) (2023) 1727, <https://doi.org/10.3390/PR11061727>.
- [73] Y. Zhang, K.N. McPhedran, M. Gamal El-Din, Pseudomonads biodegradation of aromatic compounds in oil sands process-affected water, Sci. Total Environ. 521–522 (2015) 59–67, <https://doi.org/10.1016/J.SCITOTENV.2015.03.068>.
- [74] M.N.A. Meshref, P. Chelme-Ayala, M. Gamal El-Din, Fate and abundance of classical and heteroatomic naphthenic acid species after advanced oxidation processes: Insights and indicators of transformation and degradation, Water Res 125 (2017) 62–71, <https://doi.org/10.1016/J.WATRES.2017.08.007>.
- [75] N. Wang, P. Chelme-Ayala, L. Perez-Estrada, E. Garcia-Garcia, J. Pun, J.W. Martin, M. Belosevic, M. Gamal El-Din, Impact of ozonation on naphthenic acids speciation and toxicity of oil sands process-affected water to *vibrio fischeri* and mammalian immune system, Environ. Sci. Technol. 47 (2013) 6518–6526, https://doi.org/10.1021/ES4008195/SUPPL_FILE/ES4008195_SI_001.PDF.
- [76] G.F. Whale, M. Hjort, C. Di Paolo, A.D. Redman, J.F. Postma, J. Legradi, P.E. G. Leonards, Assessment of oil refinery wastewater and effluent integrating bioassays, mechanistic modelling and bioavailability evaluation, Chemosphere 287 (2022) 132146, <https://doi.org/10.1016/J.CHEMOSPHERE.2021.132146>.
- [77] D.C.C. da, S. Medeiros, P. Chelme-Ayala, M. Gamal El-Din, Sludge-based activated biochar for adsorption treatment of real oil sands process water: selectivity of naphthenic acids, reusability of spent biochar, leaching potential, and acute toxicity removal, Chem. Eng. J. 463 (2023) 142329, <https://doi.org/10.1016/J.CEJ.2023.142329>.
- [78] X. Li, M. Ma, W. Qi, D. Wang, Y. Han, X. Ji, K. Zhu, N. Li, In Vitro multibiomarker approaches for assessing the immunotoxicity of certain sections in yangtze river, ACS Environ. Sci. Technol. Water 2 (2022) 385–394, https://doi.org/10.1021/ACSESTWATER.1C00252/ASSET/IMAGES/LARGE/EW1C00252_0008.JPEG.
- [79] V.W. Makene, E.J. Pool, The assessment of inflammatory activity and toxicity of treated sewage using RAW264.7 cells, Water Environ. J. 29 (2015) 353–359, <https://doi.org/10.1111/WEJ.12127>.
- [80] S. Paul, N.A.S. Hussain, D.M.E. Lillico, M.A. Suares, S.O. Ganiyu, M. Gamal El-Din, J.L. Stafford, Examining the immunotoxicity of oil sands process affected waters using a human macrophage cell line, Toxicology 500 (2023), <https://doi.org/10.1016/J.TOX.2023.153680>.
- [81] T. Brzicova, E. Javorkova, K. Vrbova, A. Zajicova, V. Holan, D. Pinkas, V. Philimonenko, J. Sikorova, J. Klema, J. Topinka, P. Rossner, Molecular responses in THP-1 macrophage-like cells exposed to diverse nanoparticles, Nanomaterials 9 (2019), <https://doi.org/10.3390/NANO9050687>.

- [82] J.R. Marentette, R.A. Frank, L.M. Hewitt, P.L. Gillis, A.J. Bartlett, P. Brunswick, D. Shang, J.L. Parrott, Sensitivity of walleye (*Sander vitreus*) and fathead minnow (*Pimephales promelas*) early-life stages to naphthenic acid fraction components extracted from fresh oil sands process-affected waters, *Environ. Pollut.* 207 (2015) 59–67, <https://doi.org/10.1016/J.ENVPOL.2015.08.022>.
- [83] C. Li, L. Fu, J. Stafford, M. Belosevic, M. Gamal El-Din, The toxicity of oil sands process-affected water (OSPW): a critical review, *Sci. Total Environ.* 601–602 (2017) 1785–1802, <https://doi.org/10.1016/J.SCITOTENV.2017.06.024>.
- [84] P. Mohseni, N.A. Hahn, R.A. Frank, L.M. Hewitt, M. Hajibabaei, G. Van Der Kraak, Naphthenic acid mixtures from oil sands process-affected water enhance differentiation of mouse embryonic stem cells and affect development of the heart, *Environ. Sci. Technol.* 49 (2015) 10165–10172, <https://doi.org/10.1021/ACS.EST.5B02267>.
- [85] D.M.E. Lillico, N.A.S. Hussain, Y.Y. Choo-Yin, R. Qin, Z.T. How, M.G. El-Din, J. L. Stafford, Using immune cell-based bioactivity assays to compare the inflammatory activities of oil sands process-affected waters from a pilot scale demonstration pit lake, *J. Environ. Sci.* 128 (2023) 55–70, <https://doi.org/10.1016/J.JES.2022.07.018>.
- [86] What are the oil sands?, (n.d.). (<https://natural-resources.canada.ca/our-natural-resources/energy-sources-distribution/fossil-fuels/crude-oil/what-are-oil-sands/18089>) (accessed April 16, 2024).
- [87] Canadian Climate Normals - Climate - Environment and Climate Change Canada, (n.d.). (https://climate.weather.gc.ca/climate_normals/index_e.html) (accessed April 16, 2024).